Geomechanics and Engineering, *Vol. 29, No. 4 (2022) 407-420*
https://doi.org/10.12989/gae.2022.29.4.407

Load–settlement curve combining base and shaft resistance considering curing of cement paste

Mi Jeong Seo[1a], Jong-Bae Park[2b], Dongsoo Lee[1c] and Jong-Sub Lee*[1]

[1]*School of Civil, Environmental and Architectural Engineering, Korea University, 145, Anam-ro, Seongbuk-gu, Seoul, 02841, Republic of Korea*
[2]*Land and Housing Institute, Korea Land & Housing Corporation, 99, Expo-ro 539beon-gil, Yuseong-gu, Daejeon, 34047, Republic of Korea*

(Received January 2, 2022, Revised April 8, 2022, Accepted April 10, 2022)

Abstract. Embedded piles, which are typically used in Korea, are precast piles inserted into prebored ground with cement paste. Dynamic pile tests tend to underestimate the bearing capacity of embedded piles because of the undeveloped shaft resistance prior to the curing of the cement paste and the insufficient energy transferred after the curing. In this study, a resistance combination method using the base resistance before the cement paste is cured and the shaft resistance after the cement paste is cured is proposed to obtain a combined load–settlement curve from dynamic pile tests. Two pairs of embedded piles with diameters of 600 and 500 mm are installed. Each pair comprises one pile for the dynamic pile test and another pile for the static load test. The shape of the load–settlement curve obtained using the proposed method is similar to that obtained from the static load test. Thus, the resistances evaluated using the proposed method at selected settlements are similar to those obtained from the static load test. This study shows that the resistance combination method may be used effectively in dynamic pile tests to accurately evaluate the bearing capacity of embedded piles.

Keywords: base resistance; dynamic pile test; embedded pile; load–settlement curve; shaft resistance

1. Introduction

Most pile foundations in Korea are installed using the embedded pile method to minimize noise and vibration during installation (Park 2017, Hong and Chai 2003, 2005). An embedded pile is a precast pile inserted into the ground with injection of cement paste after boring. The separated doughnut auger (SDA) method is typically used to install embedded piles. The construction process of the SDA method is illustrated in Fig. 1. In the SDA method, the ground is first bored using a counter-rotating auger and casing, as shown in Fig. 1(a). To obtain a sufficient bearing capacity, the borehole is designed to reach a stiff layer, such as weathered rock, as shown in Fig. 1(b). After the boring is completed, the casing remains in the ground and the auger is removed, as shown in Fig. 1(c). A precast pile is inserted into the borehole, as shown in Fig. 1(d). Pretensioned spun high strength concrete (PHC) and steel pipe piles are typically used as precast piles. When the pile base reaches the end of the borehole, cement paste is injected and the casing is pulled out, as shown in Fig. 1(e). Cement paste can be injected into the space between the hole and pile. Note that the casing diameter is typically 50–100 mm larger than the pile diameter. The pile is fixed in place via hammer blowing or pressing, as shown in Fig. 1(f) (Hong and Chai 2003, 2005). Cement paste significantly affects the pile capacity of the embedded pile method. Note that the cement paste increases the end bearing capacity of the embedded pile by mixing with slime, which is formed near the pile base by loosened soils and water during boring (Hong and Chai 2003, 2005). In addition, the skin friction of the embedded pile is generated by curing the cement paste (Hong and Chai 2003, 2005).

Dynamic pile tests (DPTs) are typically performed to evaluate the bearing capacity of embedded piles. DPTs are typically conducted on embedded piles prior to curing the cement paste (DPT-BC) or after curing the cement paste (DPT-AC). DPT-BC is conducted immediately after pile installation, whereas the DPT-AC is conducted when the injected cement paste is sufficiently cured (Park 2017). A comparison of the bearing capacity characteristics of the DPT-BC and DPT-AC on the embedded pile is shown in Fig. 2. Fig. 2(a) shows that skin friction does not develop during the DPT-BC because the cement paste is not cured. After the cement paste is sufficiently cured, skin friction develops. Thus, skin friction is evaluated using the DPT-AC. Despite the increase in total resistance, the DPT-BC and DPT-AC are typically conducted on the embedded piles using the same hammer, which is adopted for blowing during pile installation, as shown in Fig. 1(f). During the DPT-AC, the energy transferred to the pile base is considerably less than that applied to the pile head, due to the increase in skin friction. Therefore, the end bearing capacity may be underestimated by the DPT-AC if the

*Corresponding author, Professor
E-mail: jongsub@korea.ac.kr
[a]Ph.D. Candidate
[b]Ph.D.
[c]Ph.D. Candidate

ISSN: 2005-307X (Print), 2092-6219 (Online)

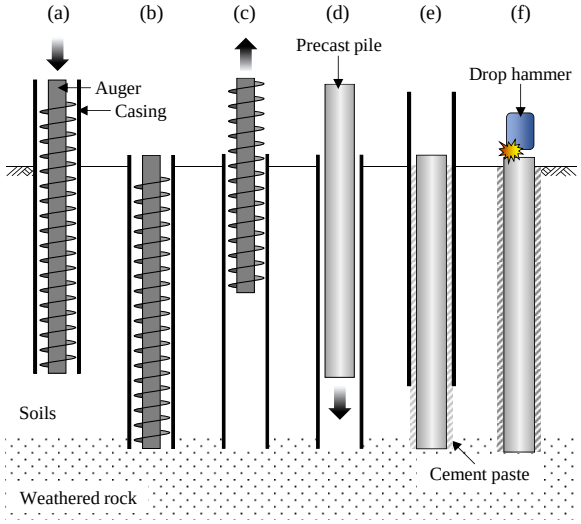

Fig. 1 Embedded pile construction using separated doughnut auger method: (a) boring with auger and casing, (b) reaching bearing stratum, (c) pulling out auger, (d) inserting precast pile, (e) injecting cement paste and pulling out casing and (f) finishing with blow (modified from Seo *et al*. (2021))

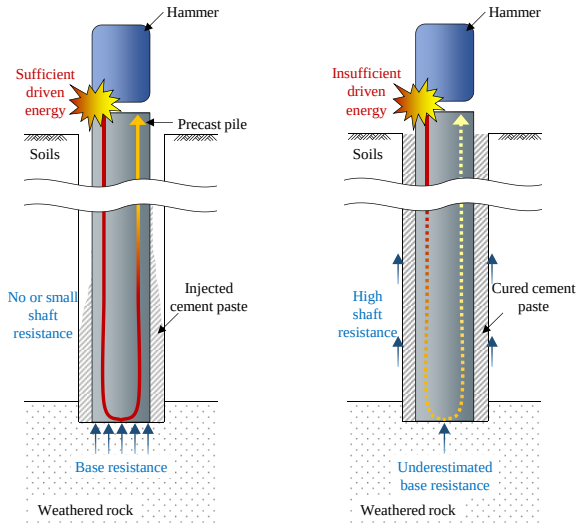

(a) Before curing of cement paste (b) After curing of cement paste

Fig. 2 Comparison of bearing capacity characteristics of embedded pile

transferred energy is not sufficient to fully mobilize the end bearing capacity as shown in Fig. 2(b) (Park 2017). Comparison tests between DPTs and static load tests on embedded PHC piles show that the bearing capacities evaluated using static load tests are approximately 30% greater than those evaluated using the DPT-AC due to the limited hammer size (Park 2017).

As skin friction is not developed during the DPT-BC, and the base resistance is not fully mobilized during the DPT-AC, the bearing capacities of the embedded piles are typically underestimated by the DPT. To account for the underestimated bearing capacity, a reduced safety factor (2.0 to 1.75) was suggested. In addition, Park (2017) suggested a simple summation method, which is the summation of the base resistance estimated during the DPT-BC and the shaft resistance obtained during the DPT-AC. Although Park's simple summation increased the pile capacities, it did not yield load–settlement curves. A load–settlement curve should be obtained to apply the criteria for evaluating the resistances and corresponding safety factors (Poulos and Davis 1968, Randolph and Wroth 1978, Fellenius 1980, Hirayama 1990, Murakami 2019). Several studies have focused on the load transfer mechanism in pile foundations to obtain the load–settlement curve. Coyle and Reese (1966) suggested that the load–settlement curve at the pile head may theoretically be estimated using the load transfer mechanism. Lee and Park (2008) analyzed bidirectional load test results based on the load transfer mechanism to consider the elastic deformation of piles.

The objective of this study is to develop a resistance combination method for embedded piles using the base resistance obtained during the DPT-BC and the shaft resistance estimated during the DPT-AC. Note that the proposed method yields a load–settlement curve at the pile head. Two pairs of test piles are installed using the SDA method. Each pair comprises a pile for the DPT and another pile for the static load test. The DPT-BC and DPT-AC results are analyzed using the Case pile wave analysis program (CAPWAP) (Pile Dynamics Inc. 2014). The combined resistance and load–settlement curves at the pile head are obtained using the proposed method. Finally, the results of the resistance combination method are analyzed and compared with those of the static load test.

2. Resistance combination method

2.1 Load transfer mechanisms in piles

For the computation of the load–settlement curve by combining the base resistance before curing of the cement paste and shaft resistance after curing the cement paste, the load transfer mechanism represented in Fig. 3 is used. The pile is divided into several segments as shown in Fig. 3(a). The load transfer curve of a pile refers to the transferred load at each segment (P_1, P_2, …, P_N) according to the depth as shown in Fig. 3(b). The load–settlement curves at the top of each segment are plotted in Fig. 3(c). First, the top resistance of Segment 1 (P_1) corresponds to the load applied to the pile head (P_T) as shown in Figs. 3(b) and 3(c). For Segment 1, the P_1 is resisted by the shaft resistance (SF_1) and bottom resistance (B_1). As the P_1 is applied to the top of Segment 1, Segment 1 settles by the top settlement (s_1), which is the summation of the elastic deformation (δ_1) and net settlement (n_1), as shown in Fig. 3(c). The net settlement of Segment 1 (n_1) becomes the top settlement of Segment 2 (s_2). The bottom resistance of Segment 1 (B_1) corresponds to the load applied to the top of Segment 2 (P_2). Second, for Segment 2, the P_2 (= B_1) is resisted by the shaft resistance (SF_2) and bottom resistance (B_2) as shown in Figs. 3(b) and 3(c). The top settlement of Segment 2 (s_2) includes the elastic deformation (δ_2) and net settlement (n_2). Third, for Segment i, the load applied to the top (P_i) is supported by

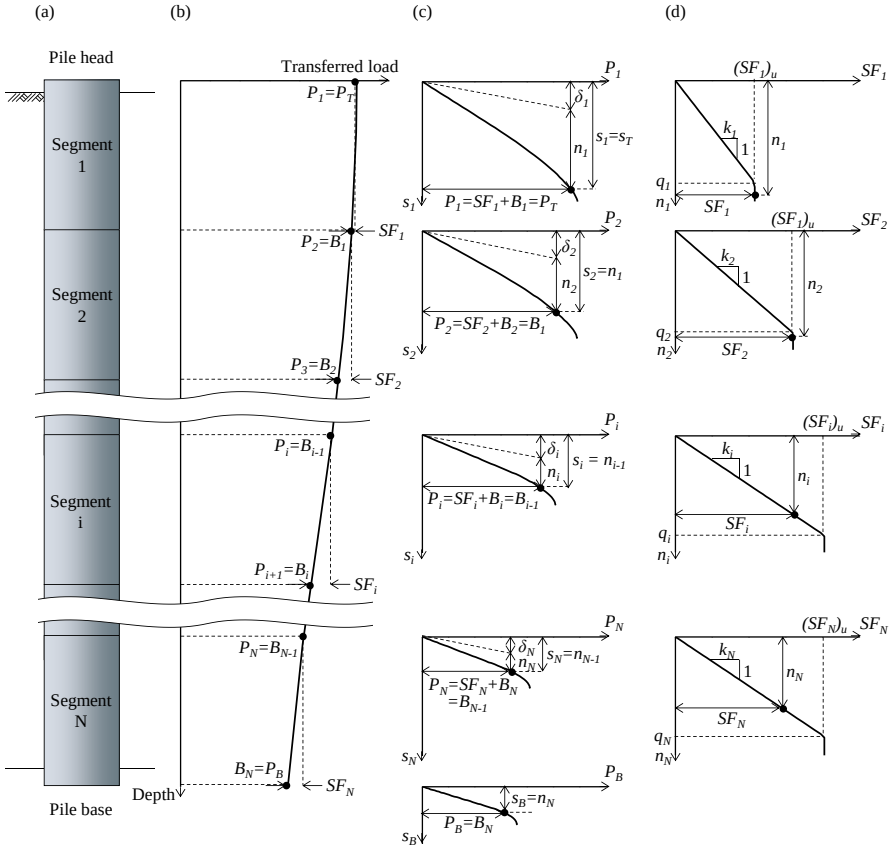

Fig. 3 Load transfer mechanism for resistance combination method: (a) pile segment, (b) load transfer curve, (c) load–settlement curves at each segment head and (d) shaft resistance models

P_i, SF_i, and B_i represent the top, shaft, and base resistance, respectively, of the Segment i. s_i, δ_i, and n_i represent the top settlement, elastic shortening, and net settlement of the Segment i, respectively. q_i, k_i, and $SF_{u,i}$ represent the shaft quake, soil stiffness, and ultimate shaft resistance of the Segment i, respectively. P_T and s_T represent the applied load at the pile head and total settlement, respectively. P_B and s_B represent the base resistance and settlement of the pile, respectively

the shaft resistance (SF_i) and bottom resistance (B_i) as shown in Fig. 3(c). Hence, Segment i settles by s_i, which is the summation of the elastic deformation (δ_i) and net settlement (n_i). Note that the elastic deformation (δ_i) of Segment i is calculated as follows

$$\delta_i = \frac{0.5(P_i + B_i) \times L_i}{E_i \times A_i} \quad (1)$$

where δ_i, P_i and B_i are the elastic deformation, top and bottom resistances of Segment i, respectively. L_i, E_i, and A_i represent the length, elastic modulus, and cross-sectional area of Segment i, respectively. Note that the skin friction at each segment is assumed to be uniform. The bottom resistance (B_i) and net settlement (n_i) of Segment i become the load applied to the top (P_{i+1}) and corresponding top settlement (s_{i+1}) of Segment (i+1). Lastly, for Segment N, the bottom resistance (B_N) and net settlement (n_N) become the base resistance (P_B) and base settlement (s_B) of the pile as shown in Figs. 3(b) and 3(c).

2.2 Computation of load transfer curve

The load transfer curves estimated by the dynamic pile tests (DPTs) conducted before and after curing of the cement paste (DPT-BC and DPT-AC, respectively) and the load combination method at the maximum loading step are shown in Figs. 4(a)-4(c), respectively. Note that the first and second subscripts in Q_{12} refer to the resistance type (T: total resistance; B: base resistance; S: shaft resistance) and evaluation method (B: DPT-BC; A: DPT-AC; C: resistance combination method), respectively. For example, Q_{TB} represents the total resistance evaluated by the DPT-BC. Fig. 4(a) shows that the maximum total resistance (Q_{TB}) is the summation of the maximum base resistance (Q_{BB}) and maximum shaft resistance (Q_{SB}) obtained from the DPT-BC ($Q_{TB} = Q_{BB} + Q_{SB}$). The Q_{BB} provides most of the Q_{TB} because the cement paste injected during pile installation is not cured. Fig. 4(b) shows that the maximum total resistance after curing of the cement paste (Q_{TA}) is the summation of the maximum base resistance (Q_{BA}) and maximum shaft resistance (Q_{SA}) obtained from the DPT-AC ($Q_{TA} = Q_{BA} + Q_{SA}$). During the DPT-AC on embedded piles, Q_{BA} is typically underestimated if the hammer capacity is not enough to fully displace the pile base. The combined load transfer curve for this method is presented in Fig. 4(c), which shows that the total combined resistance by this method (Q_{TC}) is the summation of the maximum base resistance (Q_{BB}) from the DPT-BC and maximum shaft resistance (Q_{SA}) from the DPT-AC ($Q_{TC} = Q_{BB} + Q_{SA}$). Thus, the shaft resistance (Q_{SA}) in the combined load

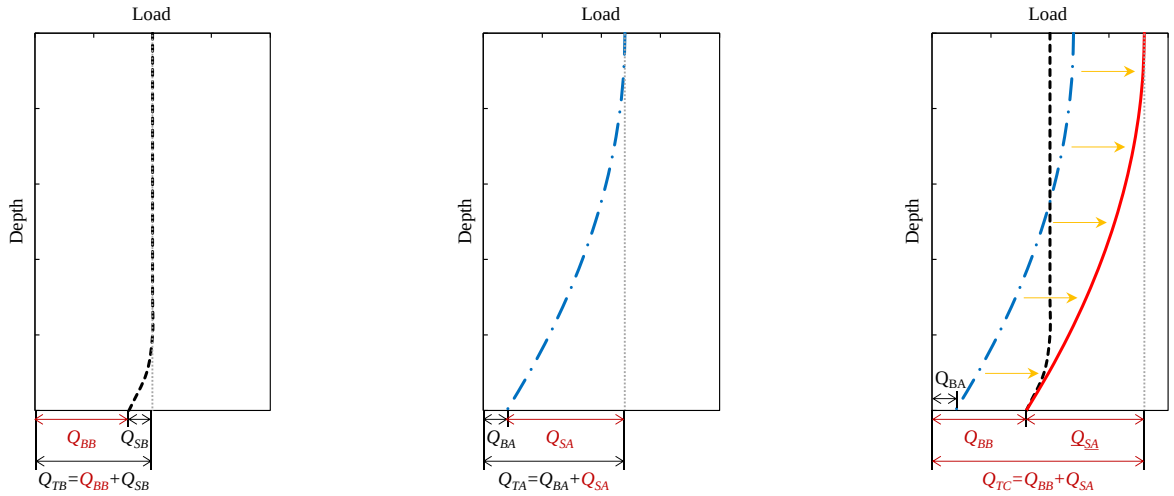

(a) Dynamic pile test before curing of cement paste (DPT-BC)

(b) Dynamic pile test after curing of cement paste (DPT-AC)

(c) Resistance combination method at maximum load

Fig. 4 Load transfer curve

Q_{BB}, Q_{SB}, and Q_{TB} represent the base, skin, and total resistance evaluated before curing of the cement paste, respectively. Q_{BA}, Q_{SA}, and Q_{TA} represent the base, skin, and total resistance evaluated after curing of the cement paste, respectively. Q_{TC} represent the total resistance by the combination method

transfer curve moves in parallel from the Q_{BA} point to the Q_{BB} point at the pile base as shown in Fig. 4(c).

2.3 Computation of load–settlement curve

The load–settlement curves at the pile heads and bases, and load transfer curves under the maximum load from the DPT-BC and DPT-AC can be obtained using the Case pile wave analysis program (CAPWAP) (Pile Dynamics Inc. 2014). Note that in the proposed method, the shaft resistance at each segment is determined by the net settlement at the segment bottom as shown in Fig. 3(d). That is, the shaft resistance of Segment i (SF_i) is calculated as follows (Pile Dynamics Inc. 2014)

$$SF_i = \begin{cases} k_i \times n_i & \text{for } n_i < q_i \\ (SF_i)_u & \text{for } n_i \geq q_i \end{cases} \quad (2)$$

where k_i, q_i, and $(SF_i)_u$ represent the soil stiffness, shaft quake, and ultimate shaft resistance of Segment i, respectively. For the computation of the load–settlement curve using this method, the shaft resistance parameters, which are k_i, q_i, and $(SF_i)_u$ shown in Fig. 3(d), of the DPT-AC are required. First, for Segment N under the maximum load of the DPT-AC, the n_N (= s_B) is known from the load–settlement curve at the pile base as shown in Fig. 3(c). Moreover, the P_N is known from the load transfer curve as shown in Fig. 3(b). Thus, the SF_N is calculated as the P_N by subtracting the B_N. As the shaft quake of Segment N (q_N) is the soil property for the CAPWAP analyses, the soil stiffness of Segment N (k_N) is estimated using Eq. (2). The total settlement of Segment N (s_N) is the summation of the n_N and δ_N, which is calculated using Eq. (1). Next, for Segment (N-1) under the maximum load, the n_{N-1} and B_{N-1} correspond to the s_N and P_N, respectively. The SF_{N-1} is calculated using the P_{N-1}, which is known from the load transfer curve as shown in Fig. 3(b), and B_{N-1}. Thus, the k_{N-1} is determined by the SF_{N-1} and q_{N-1} using Eq. (2). Thus, the soil stiffnesses of all segments can be determined using the same process from Segment N to Segment 1.

After the soil stiffnesses of all segments are determined at the maximum loading step, the load–settlement curve can be obtained by computing the load and settlement of all segments at all loading steps. First, for Segment N at the first loading step, the bottom resistance ($B_{N,1}$) and net settlement ($n_{N,1}$) are the same as the pile base resistance ($P_{B,1}$) and settlement ($s_{B,1}$), respectively, which are known from the load–settlement curve at the pile base. Then, from the $n_{N,1}$, q_N, and k_N, the shaft resistance ($SF_{N,1}$) is determined using Eq. (2). The top resistance ($P_{N,1}$) is obtained by the summation of the $B_{N,1}$ and $SF_{N,1}$ ($P_{N,1} = B_{N,1} + SF_{N,1}$). In addition, the elastic deformation ($\delta_{N,1}$) is calculated using Eq. (1). Consequently, the top settlement ($s_{N,1}$) is obtained by the summation of the $n_{N,1}$ and $\delta_{N,1}$ ($s_{N,1} = n_{N,1} + \delta_{N,1}$). Next, for Segment (N-1) at the first loading step, the bottom resistance ($B_{N-1,1}$) and net settlement ($n_{N-1,1}$) correspond to the $P_{N,1}$ and $s_{N,1}$. In addition, the shaft resistance ($SF_{N-1,1}$) is calculated using the $n_{N-1,1}$, q_{N-1}, and k_{N-1} in Eq. (2). Then, the top resistance ($P_{N-1,1}$) is obtained by the summation of the $B_{N-1,1}$ and $SF_{N-1,1}$ ($P_{N-1,1} = B_{N-1,1} + SF_{N-1,1}$). After the process is repeated from Segment N to Segment 1 at the first loading step, the total resistance and settlement of the pile, which correspond to the top resistance ($P_{1,1}$) and settlement ($s_{1,1}$) of Segment 1, are obtained. Finally, the top resistances and settlements of all segments at all loading steps can be obtained using the same process as the loading step increases. Thus, the top resistances (P_1) and settlements (s_1) of Segment 1 at all loading steps become the load–settlement curve at the pile head.

Table 1 Test pile information

Test pile		PHC pile Diameter [mm]	Thickness [mm]	Cross-sectional area [m^2]	Elastic modulus [GPa]	Length [m]	Inclined base plate diameter [mm]	Hole diameter [mm]	Test	Test date after pile installation
TP-1	TP-1D	600	90	0.1442	39.2	13.9	-	682	DPT-BC	Immediately
									DPT-AC	29 days
	TP-1S	600	90	0.1442	39.2	13.8	-	682	Static load test	21 days
TP-2	TP-2D	500	80	0.1056	39.2	13.2	560	682	DPT-BC	Immediately
									DPT-AC	28 days
	TP-2S	500	80	0.1056	39.2	12.3	560	682	Static load test	25 days

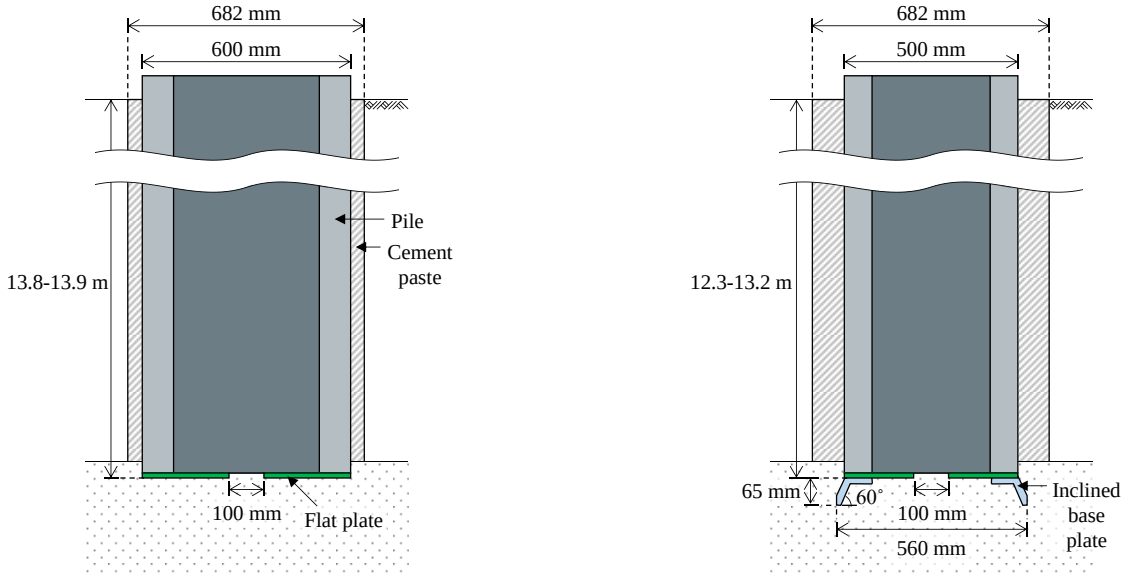

(a) TP-1 (b) TP-2

Fig. 5 Schematics of test piles

2.4 Limitation of resistance combination method

This study suggests the resistance combination method, which is based on the load–settlement curve at the pile base obtained by the DPT-BC and shaft resistance parameters (k_i, q_i, and $(SF_i)_u$) obtained by the DPT-AC. In general, the CAPWAP analysis includes more uncertainties for embedded piles than driven piles, as the pile and soils are difficult to be modeled. The proposed method simply uses the CAPWAP results from the DPT-BC and DPT-AC without any modification, provided that the results of the DPT are appropriate. Thus, the resistance combination method has the limitation, which is the inherent uncertainties in modelling an embedded pile using the CAPWAP. In addition, the behavior of the interface between the nondisplacement pile and soils is known to be non-elastic (Zhang *et al*. 2019, Li *et al*. 2017, Mascarucci *et al*. 2014, Lashkari 2013, Rollins *et al*. 2005). In the proposed method, however, the relationship between the shaft resistance and net settlement at each segment is supposed to be elasto-plastic as shown in Fig. 3(d). The limitations of this method may be confirmed and analyzed with further studies.

3. Experimental setup

3.1 Test piles

Four piles were installed using the separated doughnut auger (SDA) method as summarized in Table 1. The diameters of TP-1 piles, including TP-1D and TP-1S were 600 mm, whereas those of TP-2 piles, including TP-2D and TP-2S were 500 mm. For TP-1 piles, the cross-sectional area was 0.1442 m^2, as the pile thickness was 90 mm. For TP-2 piles, the cross-sectional area was 0.1056 m^2, as the thickness of TP-2 was 80 mm. The four piles were pretensioned spun high strength concrete (PHC) piles with the compressive strength of 110 MPa. The elastic modulus of the four PHC piles was 39.2 GPa as summarized in Table 1. The lengths of TP-1D, TP-1S, TP-2D, and TP-2S were 13.9, 13.8, 13.2, and 12.3 m, respectively. TP-1 piles (TP-1D and TP-1S) and TP-2 piles (TP-2D and TP-2S) are compared in Fig. 5. TP-1 piles were typical piles with a flat plate attached to the base as shown in Fig. 5(a). An inclined base plate with the diameter of 560 mm was attached to the base of TP-2 piles as shown in Fig. 5(b) (see details in Seo

Table 2 Dynamic pile test information

Test pile	Test	Hammer type	Ram weight [kN]	Drop height [m]	SET[a] [mm/blow]	EMX[b] [kJ]	FMX[c] [kN]	RMX[d] [kN]
TP-1D	DPT-BC	Drop	58.9	2.5	5.0	57.6	3636	3460
	DPT-AC	Hydraulic	98.1	0.5	0.1	16.1	2381	2144
				0.9	6.0	58.1	5932	3619
TP-2D	DPT-BC	Drop	58.9	2.0	1.0	43.3	2579	3857
	DPT-AC	Hydraulic	98.1	0.7	1.0	46.6	4271	3841

[a] SET: Set value
[b] EMX: Maximum transferred energy measured from the gauges
[c] FMX: Maximum compressive force measured at the gauges
[d] RMX: Capacity evaluated by the Case method with the Case damping factor of 0.5

et al. 2021, 2019, Han *et al*. 2020). The hole diameter is supposed to be approximately 682 mm, which corresponds to the outer diameter of the casing as shown in Fig. 5.

3.2 Test setup

The layout of the test piles is presented in Fig. 6. Fig. 6(a) shows that TP-1D, TP-1S, TP-2S, and TP-2D were installed in a row. The ground anchors were installed on both sides of TP-1S and TP-2S to conduct static load tests. A standard penetration test (SPT) was conducted at the center of the test piles. High strain dynamic tests (ASTM D4945), which are known as DPTs, were conducted on TP-1D and TP-2D. The DPT-BC of TP-1D and TP-2D was conducted immediately after pile installation. In addition, the DPT-AC of TP-1D and TP-2D was conducted 29 and 28 days after pile installation, respectively, as summarized in Table 1. Information on the DPT-BC and DPT-AC is presented in Table 2. A drop hammer with the ram weight of 58.9 kN was used during the DPT-BC, whereas a hydraulic hammer with the ram weight of 98.1 kN was used during the DPT-AC for both TP-1D and TP-2D. For TP-1D, the drop height of the DPT-BC was 2.5 m. The set value (SET) observed during the DPT-BC was 5.0 mm/blow. The maximum transferred energy measured from the gauges (EMX) was 57.6 kJ. During the DPT-AC of TP-1D, as the drop height increases from 0.5 to 0.9 m, SET increases from 0.1 to 6.0 mm/blow. In addition, the EMX increases from 16.1 to 58.1 kJ. For TP-2D, the drop height of 2.0 m, and EMX was 43.3 kJ during the DPT-BC. The EMX measured during the DPT-AC at the drop height of 0.7 m was 46.6 kJ, which is similar to that during the DPT-BC. Both SETs observed during the DPT-BC and DPT-AC were 1.0 mm/blow.

Static axial compressive load tests (ASTM D1143), which are known as static load tests, were conducted on TP-1S and TP-2S. The static load tests were performed using the quick method, where the load was applied to the pile head using hydraulic jacks and a reaction anchor system as represented in Fig. 6. The load and settlement at the pile head were measured using a loadcell and linear variable differential transducers. The static load tests of TP-1S and TP-2S were conducted 21 and 25 days after pile installation, respectively, as summarized in Table 1.

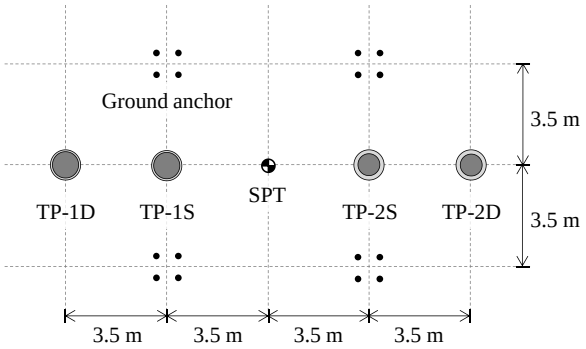

Fig. 6 Test pile arrangement

Note that pile diameter of TP-1D and TP-1S is 600 mm and that of TP-2D and TP-2S is 500 mm. The hole diameter of all test piles is 682 mm

Table 3 Grain size properties of soils along the depth

Sampled depth [m]	Median diameter, D_{50} [mm]	Gradation coefficient, C_c	Uniformity coefficient, C_u	USCS*
2.3	1.04	1.34	3.23	SP
4.3	1.29	1.07	2.23	SP
7.3	1.12	0.47	0.81	SP
10.3	1.10	1.13	2.43	SP
13.3	0.99	0.80	1.43	SP

* Unified soil classification system

A standard penetration test (SPT) was conducted to determine the ground conditions at the middle of the test piles as shown in Fig. 6. SPT N-values were measured, and the soils were sampled every 1 m. The distribution of the N-value according to the depth is plotted in Fig. 7(a). The SPT N-values of the ground within a depth of 6.3 m range from 4 to 16 blows per 30 cm. The SPT N-values of the ground below a depth of 10.3 m are greater than 50 blows per 30 cm as shown in Fig. 7(a). The SPT N-values of the weathered rock are greater than 100 blows per 30 cm. The particle size distribution curves of soils, which were sampled at depths of 2.3, 4.3, 7.3, 10.3, and 13.3 m during the SPT, are represented in Fig. 7(b). In addition, the grain size properties of soils at each depth are summarized in Table 3. The gradation coefficients (C_c) and uniformity coefficients (C_u) of soils are in the range of 0.47–1.34 and 0.81–3.23, respectively. The soils, in which the test piles were installed, are classified as poorly graded sand (SP).

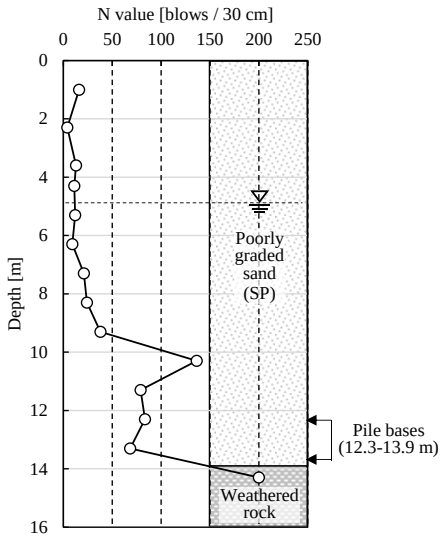

(a) SPT N-value

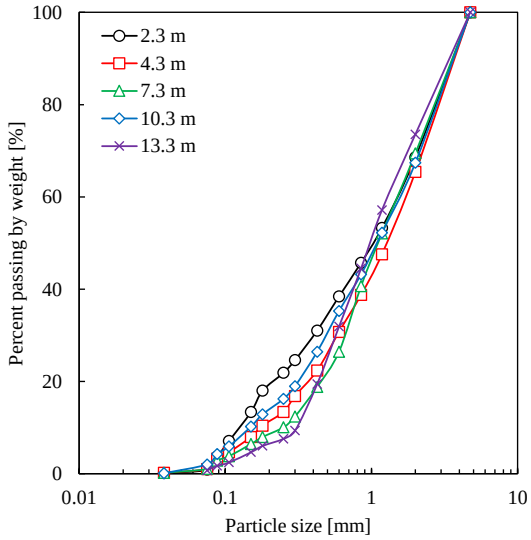

(b) Particle size distribution curve

Fig. 7 Results of site characterization according to depth

4. Experimental results

4.1 Force and velocity waveforms

4.1.1 TP-1D

The force and velocity waveforms, which were measured using strain gauges and accelerometers installed at the head of TP-1D, are plotted in Fig. 8. Fig. 8(a) presents the DPT-BC result with the EMX of 57.6 kJ. The degree of separation between the force and velocity waveforms in the range 0–1 in the 2L/c (where L and c represent the pile length and wave speed, respectively) implies the amount of shaft resistance. The shaft resistance is expected to be small, as Fig. 8(a) shows that the force and velocity waveforms are hardly separated for the DPT-BC. The measured data and simple analyses of the waveforms obtained using DPTs are summarized in Table 2. The maximum compressive force measured at the gauges

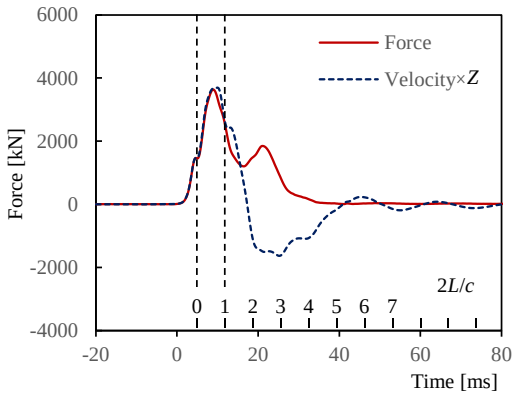

(a) Dynamic pile test before curing of cement paste (DPT-BC) with maximum transferred energy (EMX) of 57.6 kJ

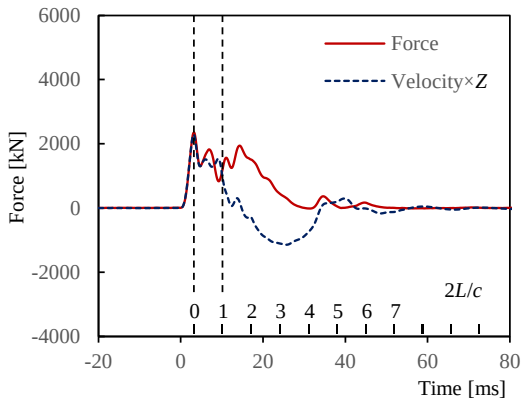

(b) Dynamic pile test after curing of cement paste (DPT-AC) with EMX of 16.1 kJ

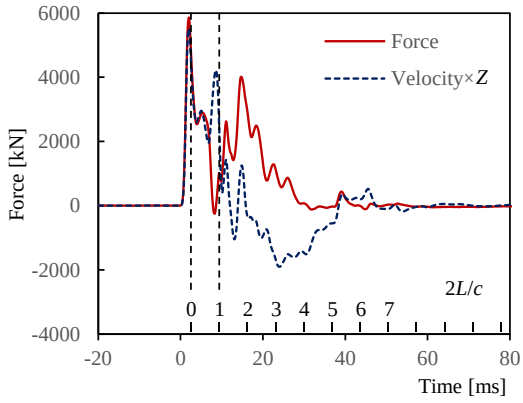

(c) DPT-AC with EMX of 58.1 kJ

Fig. 8 Force and velocity waveforms of TP-1D

Z represents the pile impedance. L and c represent the pile length and wave speed, respectively

(FMX) was 3636 kN. The capacity evaluated by the Case method with the Case damping factor of 0.5 (RMX) was 3460 kN.

As the drop height increases from 0.5 to 0.9 m during the DPT-AC of TP-1D, the EMX increases from 16.1 to58.1 kJ. The force and velocity waveforms, which were measured during the DPT-AC with the EMX of 16.1, are shown in Fig. 8(b). The force greater than the velocity

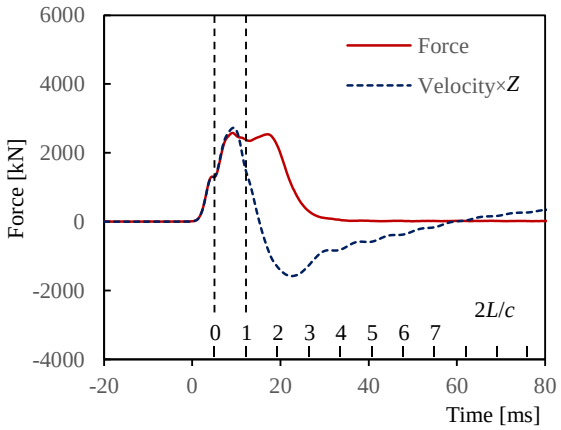

(a) Dynamic pile test before curing of cement paste (DPT-BC) with maximum transferred energy (EMX) of 43.3 kJ

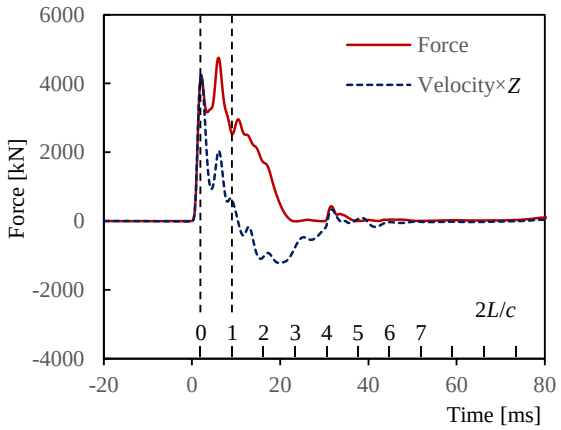

(b) Dynamic pile test after curing of cement paste (DPT-AC) with EMX of 46.6 kJ

Fig. 9 Force and velocity waveforms of TP-2D

Z represents the pile impedance. L and c represent the pile length and wave speed, respectively

within 0.5 in the 2L/c indicates the greater mobilized shaft resistance. The measured data and simple analyses of the waveforms are summarized in Table 2. For the DPT-AC with the EMX of 16.1 kJ, the FMX and RMX were 2381 and 2144 kN, respectively. The force and velocity waveforms measured during the DPT-AC with the EMX of58.1 kJ are shown in Fig. 8(c). The shaft resistance is not detected, because the force and velocity waveforms are not separated as shown in Fig. 8(c). For the DPT-AC with the EMX of 58.1 kJ, the FMX and RMX were 5932 and 2381 kN, respectively, as summarized in Table 2. For the DPT-AC of TP-1D, the RMX increases from 2144 to 3619 kN, as the EMX increases from 16.1 to 58.1 kJ. Note that the shaft resistance may decrease as the cement paste, which is injected into the space between the hole and PHC pile, may be broken with increasing EMX.

4.1.2 TP-2D

The force and velocity waveforms measured during the DPT-BC of TP-2D are plotted in Fig. 9(a). Fig. 9(a) shows that the force and velocity waveforms are hardly separated in the range of 0–1 in the 2L/c. Note that no separation indicates no shaft resistance before curing of the cement paste. The data obtained from the DPT-BC of TP-2D are summarized in Table 2. The RMX with the EMX of 43.3 kJ and FMX of 2579 kN was evaluated to be 3857 kN. The force and velocity waveforms measured during the DPT-AC of TP-2D are plotted in Fig. 9(b). As the force waveform rises above the velocity waveforms in Fig. 9(b), the shaft resistance is expected to be high. Table 2 shows that the RMX with the EMX of 46.6 kJ and FMX of 4271 kN evaluated by the DPT-AC of TP-2D was 3841 kN.

4.2 CAPWAP results

4.2.1 TP-1D

CAPWAP analyses were performed to obtain the load–settlement curves from the DPT results (Likins *et al*. 1996, Likins and Rausche 2004, Rausche *et al*. 2010, Pile Dynamics Inc. 2014). The shaft quakes (q_i) used for the CAPWAP analyses are in the range of 5.4 to 7.5 mm for DPT-AC. The load–settlement curves at the head and base of TP-1D obtained using the CAPWAP analyses are plotted in Figs. 10(a) and 10(b), respectively. For quantitative comparison, the maximum total resistance (Q_T), maximum base resistance (Q_B), and maximum shaft resistance (Q_S) are summarized in Table 4. Note that Q_T and Q_B are evaluated as the maximum resistance values of the load–settlement curves at the head and base, respectively. Q_S are calculated by subtracting Q_B from Q_T. Before curing of the cement paste, Q_{TB}, which refers to the maximum total resistance, was 3415 kN. Q_{BB} and Q_{SB}, which refer to the maximum base and shaft resistance of the DPT-BC, were 2982 and 433 kN, respectively. After curing of the cement paste under the EMX of 16.1 kJ, Q_{TA}, which refers to the maximum total resistance, was 1896 kN. Q_{BA} and Q_{SA}, which refer to the maximum base and shaft resistance of the DPT-AC, were 1167 and 729 kN, respectively, as summarized in Table 4. For the DPT-AC with the EMX of 58.1 kJ, the Q_{TA}, Q_{BA}, and Q_{SA} were 3152, 2701, and 450 kN, respectively. For TP-1D, the Q_{TB} is greater than the Q_{TA} for both the EMX of 16.1 and 58.1 kJ as presented in Fig. 10(a) and Table 4. Fig. 10 and Table 4 show that the Q_{TA} and Q_{BA} increase as the EMX increases. As the EMX increases from 16.1 to 58.1 kJ, the Q_{SA} decreases from 729 to 450 kN, and thus the portion of the shaft resistance in the total resistance decreases from 38.4% to 14.3% (see Table 4). The shaft resistance decreases because the cement paste, which is injected into the space between the hole and PHC pile, may be broken by the increased hammer energy.

4.2.2 TP-2D

For TP-2D, the shaft quakes (q_i) ranges from 4.7 to 7.5 mm for the DPT-AC. The load–settlement curves at the head and base of TP-2D estimated by the CAPWAP are plotted in Figs. 10(a) and 10(b), respectively. The Q_T, Q_B, and Q_S evaluated from the DPT-BC and DPT-AC are summarized in Table 4. Before curing of the cement paste, the Q_{TB}, Q_{BB}, and Q_{SB} were 3881, 3602, and 279 kN, respectively. Note that even though the EMX was less for TP-2D than TP-1D, the Q_{TB} and Q_{BB} were higher for TP-2D

Table 4 Maximum resistances evaluated using CAPWAP and combination method

Test pile	Capacity [kN]	Maximum resistance*					
		Total, Q_T		Base, Q_B		Shaft, Q_S	
TP-1D	DPT-BC (EMX=57.6 kJ)	3415	(100.0%)	2982	(87.3%)	433	(12.7%)
	DPT-AC (EMX=16.1 kJ)	1896	(100.0%)	1167	(61.6%)	729	(38.4%)
	DPT-AC (EMX=58.1 kJ)	3152	(100.0%)	2701	(85.7%)	450	(14.3%)
	Combination method (EMX=16.1 kJ)	3711	(100.0%)	2982	(80.4%)	729	(19.6%)
	Combination method (EMX=58.1 kJ)	3432	(100.0%)	2982	(86.9%)	450	(13.1%)
TP-2D	DPT-BC (EMX=43.3 kJ)	3881	(100.0%)	3602	(92.8%)	279	(7.2%)
	DPT-AC (EMX=46.6 kJ)	3928	(100.0%)	1616	(41.1%)	2312	(58.9%)
	Combination method (EMX=46.6 kJ)	5913	(100.0%)	3602	(60.9%)	2312	(39.1%)

Note: The numbers in parentheses refer to the ratio of the base or shaft resistance to the total resistance. EMX refers to the maximum transferred energy.
* Maximum resistance evaluated by the CAPWAP or combination method

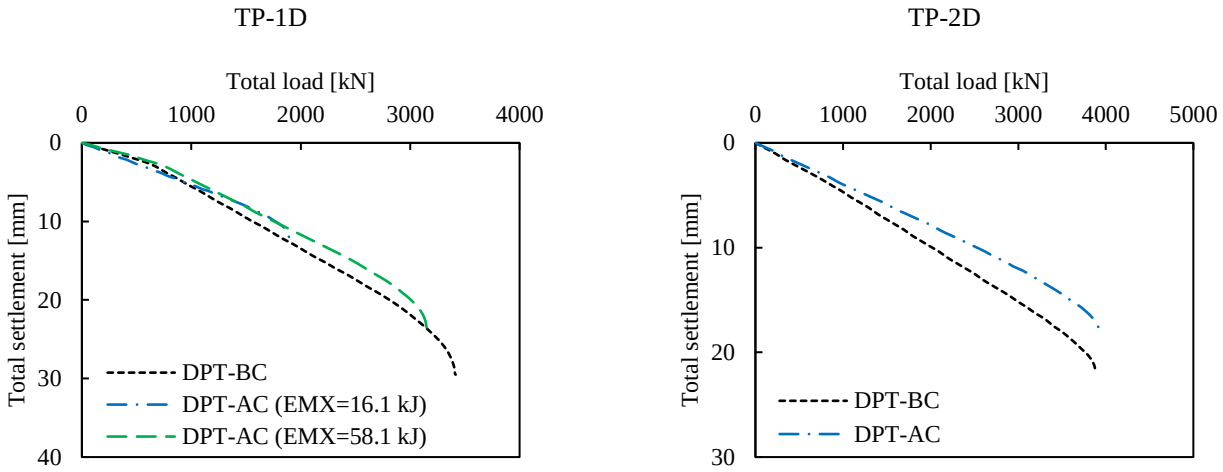

(a) Pile head

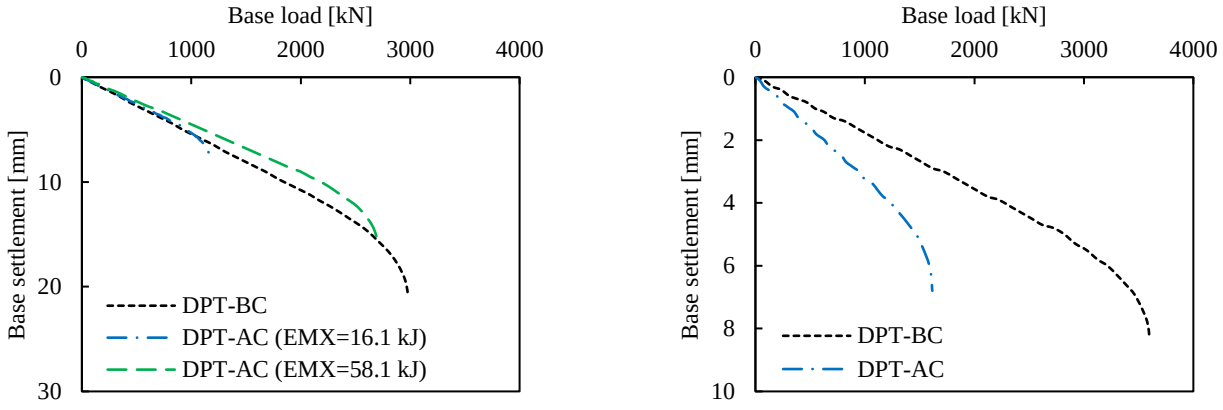

(b) Pile base

Fig. 10 Load–settlement curves estimated using CAPWAP

· DPT-BC and DPT-AC refer to the dynamic pile tests before and after curing of the cement paste, respectively.

than those for TP-1D. After curing of the cement paste, the Q_{TA}, Q_{BA} and Q_{SA} were evaluated to be 3928, 1616 and 2312 kN, respectively, as summarized in Table 4. The portion of the shaft resistance for the DPT-AC of TP-2D is 58.9%, which is greater than that for the DPT-AC of TP-1D (38.4%). For TP-2D, the Q_{TB} and Q_{TA} were similar as shown in Fig. 10(a) and Table 4. However, the stiffness of the load–settlement curve for the DPT-AC was greater than that for the DPT-BC. The greater stiffness of the load–settlement curve implies a greater shaft resistance. Thus, for

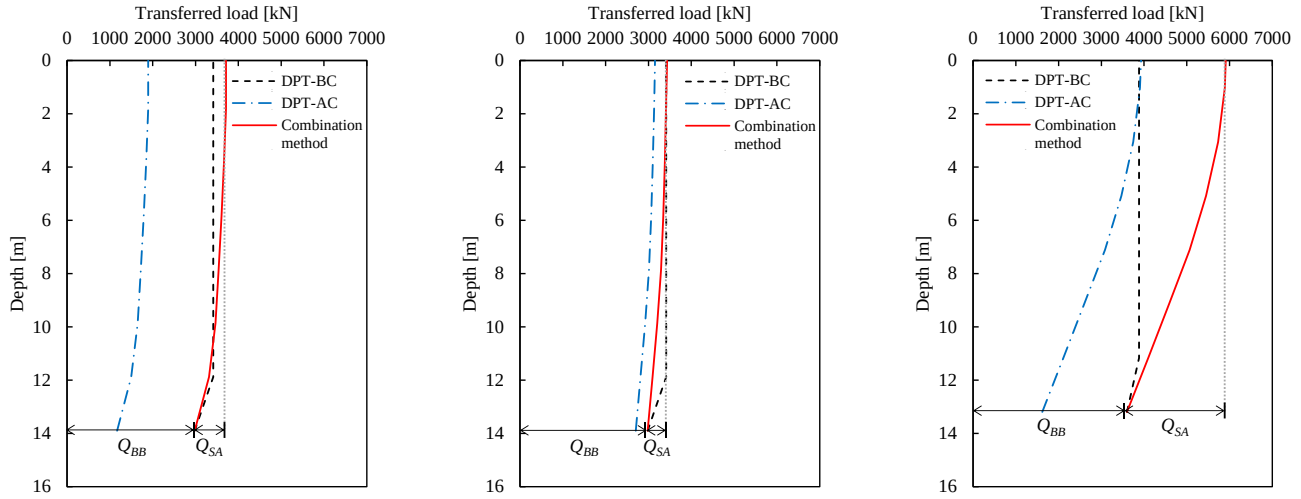

(a) TP-1D with maximum transferred energy (EMX) of 16.1 kJ during DPT-AC

(b) TP-1D with EMX of 58.1 kJ during DPT-AC

(c) TP-2D with EMX of 46.6 kJ during DPT-AC

Fig. 11 Combined load transfer curves

DPT-BC and DPT-AC refer to the dynamic pile tests before and after curing of the cement paste, respectively. Q_{BB} represents the base resistance evaluated before curing of the cement paste, and Q_{SA} represents the shaft resistance evaluated after curing of the cement paste

TP-2D, the shaft resistance was sufficiently developed after curing of the cement paste. Note that for TP-2D, the Q_{BA} (1616 kN) is considerably less than the Q_{BB} (3602 kN) as summarized in Table 4 and Fig. 10(b), because the transferred energy was not sufficient to mobilize the base resistance after curing of the cement paste.

4.2.3 Comparison between TP-1D and TP-2D

TP-1D and TP-2D had different pile base shapes and pile diameters as shown in Fig. 5. Despite the different pile diameters, the same drilling rig was adopted. Although the diameter of TP-2D (500 mm) is smaller than that of TP-1D (600 mm), the Q_{BB} of TP-2D (3602 kN) is higher than that of TP-1D (2982 kN) as summarized in Table 4. The higher Q_{BB} of TP-2D with the inclined base plate results from the increased rupture surface and greater horizontal effective stress, which implies more confinement of the soil particles (see details in Han *et al*. 2020, Seo *et al*. 2021). In addition, the Q_{SA} of TP-2D (2312 kN) is much higher than that of TP-1D (729 kN). The shaft resistance of the embedded pile is developed by curing of the cement paste, which is injected during the pile installation as described in Fig. 1. Thus, the size of the space between the hole and pile, which corresponds to the amount of the injected cement paste, is a main factor for the development of the shaft resistance. In this study, the higher Q_{SA} of TP-2D may result from the bigger space between the hole and pile as shown in Fig. 5.

5. Analyses and discussion

5.1 Combined load transfer curves

5.1.1 TP-1D

The combined load transfer curves using the base resistance before curing of the cement paste and shaft resistance after curing of the cement paste under the maximum load are plotted in Fig. 11. Note that Fig. 11 shows that the load transfer curves under the maximum load. For TP-1D, the load transfer curve, which is combined using the DPT-AC with the EMX of 16.1 kJ, is shown in Fig. 11(a). Fig. 11(a) shows that the maximum total resistance estimated by the proposed method (Q_{TC}) is the summation of the Q_{BB} and Q_{SA}. As the Q_{BB} is greater than the Q_{BA} and the Q_{SA} is greater than the Q_{SB}, the Q_{TC} is higher than the Q_{TA} and Q_{TB}. The maximum resistances evaluated using the computed load transfer curve are summarized in Table 4. As the results of this method using the DPT-AC with the EMX of 16.1 kJ, the Q_{TC} was evaluated to be 3711 kN, which is the summation of the Q_{BB} (2982 kN) and Q_{SA} (729 kN). The load transfer curve combined using the DPT-AC with the EMX of 58.1 kJ is plotted in Fig. 11(b). Fig. 11(b) shows that the Q_{TC} is almost the same as the Q_{TB} because the Q_{SA} and Q_{SB} are similar. As the results of this method using the DPT-AC with the EMX of 58.1 kJ, the Q_{TC} was evaluated to be 3432 kN, as the Q_{SA} was 450 kN as summarized in Table 4. Thus, the load transfer curve combined using the DPT-AC results with the EMX of 16.1 kJ may be more appropriate than that with the EMX of 58.1 kJ.

5.1.2 TP-2D

The combined load transfer curve computed using the DPT-BC and DPT-AC for TP-2D is plotted in Fig. 11(c). The maximum resistances evaluated using the proposed method are summarized in Table 4. The Q_{TC} of TP-2D was 5913 kN, which is the summation of the Q_{BB} (3602 kN) and Q_{SA} (2312 kN). Table 4 shows that the increase in the base resistance from the DPT-AC to DPT-BC is greater for TP-2D than for TP-1D. In addition, the increase in the shaft

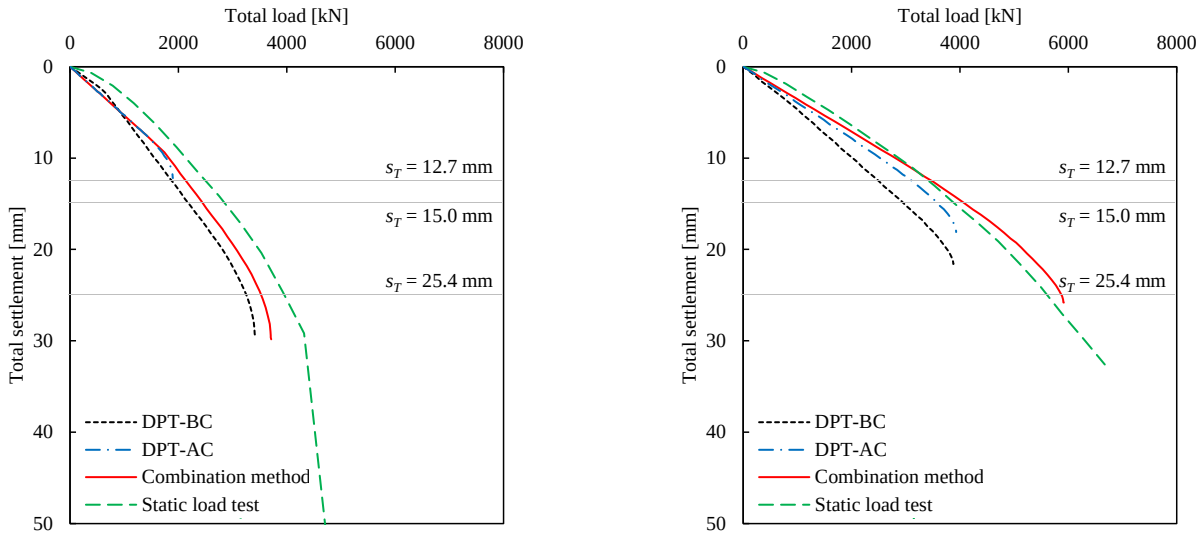

(a) TP-1 (b) TP-2

Fig. 12 Combined load–settlement curves at pile head

DPT-BC and DPT-AC refer to the dynamic pile tests before and after curing of the cement paste, respectively

resistance from the DPT-BC to DPT-AC is greater for TP-2D than for TP-1D.

5.2 Combined load–settlement curves

5.2.1 TP-1

For TP-1D, the combined load–settlement curve was computed using the load–settlement curve at the pile base (Fig. 10(b)) and load transfer curve (Fig. 11(a)). The cross-sectional area and elastic modulus of the PHC piles for the computation of the load–settlement curve are summarized in Table 1. The change in the elastic modulus due to the cement paste at each segment is also reflected in the computation. The load–settlement curves estimated by the DPT-BC, DPT-AC, and proposed method are compared in Fig. 12(a). In addition, the load–settlement curve obtained from the static load test is plotted in Fig. 12(a). Fig. 12(a) shows that the maximum total resistance estimated by the resistance combination method is greater than those by the DPT-BC and DPT-AC, yet less than that obtained from the static load test. Furthermore, the stiffness estimated from the load–settlement curve is greater for this method than for the DPT-BC and DPT-AC, yet less than that for the static load test.

For a quantitative comparison, the total resistances at the total settlements (= s_T, which corresponds to the head settlements) of 12.7, 15.0, and 25.4 mm were evaluated using Fig. 12(a). The criterion for a total settlement of 12.7 mm was suggested by Woodward (1972). The criterion based on a total settlement of 15.0 mm was used. The standards Association of Australia (AS-2159) suggests that the serviceability load is the total resistance at a total settlement of 15.0 mm. The criterion based on a total settlement of 25.4 mm is commonly used (Touma and Reese 1974, Terzaghi and Peck 1967). For TP-1, the total resistances were estimated at the s_T of 12.7, 15.0, and 25.4 mm using Fig. 12(a) as summarized in Table 5. The total resistances at the s_T of 12.7 mm estimated by the DPT-BC, proposed method, and static load test were 1904, 2162, and 2533 kN, respectively. The total resistances at the s_T of 15.0 mm were evaluated to be 2194, 2456, and 2861 kN for the DPT-BC, this method, and static load test, respectively. In addition, the total resistances at the s_T of 25.4 mm of the DPT-BC, this method, and static load test were 3287, 3553, and 3989 kN, respectively. Note that the total settlement of the DPT-AC with the EMX of 16.1 kJ was less than 12.7 mm as shown in Fig. 12(a).

The total resistances evaluated by the DPT-BC, DPT-AC, and proposed method are compared to those evaluated by static load tests to quantify the improvement achieved using the combined load–settlement curve. The ratios of the total resistances evaluated by the DPT-BC, DPT-AC, and this method to those evaluated by the static load tests are calculated, as summarized in Table 5. For TP-1, the resistances evaluated by the DPT-BC are 75.2%–82.2% of the static load test results, whereas those evaluated by this method with an EMX of 16.1 kJ are 85.4%–89.1% of the static load test results. Thus, the total resistance obtained from the proposed method is similar to those obtained from the static load test.

5.2.2 TP-2

For TP-2D, the combined load–settlement curve of the proposed method computed using Figs. 10(b) and 11(c) is plotted in Fig. 12(b). In addition, the load–settlement curves of the DPT-BC, DPT-AC, and static load test are compared in Fig. 12(b). Fig. 12(b) shows that the maximum total resistance and stiffness estimated from the load–settlement curve obtained from the resistance combination method are considerably greater than those obtained by the DPT-BC and DPT-AC. In addition, the load–settlement curve of the proposed method is virtually identical to that of the static

Table 5 Total resistances evaluated using CAPWAP, combination method, and static load test

Test pile	Capacity [kN]	Total resistance at the s_T^* of					
		12.7 mm		15.0 mm		25.4 mm	
TP-1D	DPT-BC (EMX=57.6 kJ)	1904	(75.2%)	2194	(76.7%)	3278	(82.2%)
	DPT-AC (EMX=16.1 kJ)	-	(-)	-	(-)	-	(-)
	DPT-AC (EMX=58.1 kJ)	2145	(84.7%)	2470	(86.3%)	-	(-)
	Combination method (EMX=16.1 kJ)	2162	(85.4%)	2456	(85.8%)	3553	(89.1%)
	Combination method (EMX=58.1 kJ)	1926	(76.0%)	2210	(77.2%)	3280	(82.2%)
TP-1S	Static load test	2533	(100.0%)	2861	(100.0%)	3989	(100.0%)
TP-2D	DPT-BC (EMX=43.3 kJ)	2534	(73.2%)	2969	(76.1%)	-	(-)
	DPT-AC (EMX=46.6 kJ)	3152	(91.0%)	3591	(92.0%)	-	(-)
	Combination method (EMX=46.6 kJ)	3532	(102.0%)	4095	(104.9%)	5897	(104.2%)
TP-2S	Static load test	3463	(100.0%)	3904	(100.0%)	5662	(100.0%)

Note: The numbers in parentheses refer to the ratio of the total resistance evaluated by CAPWAP or combination method to that by static load test. EMX refers to the maximum transferred energy.

* Total settlement, which corresponds to the settlement at the pile head

load test in terms of the maximum load and stiffness. However, the stiffness of this method is marginally greater than that of the static load test where the load is greater than 4000 kN, as the hole depth of TP-2D was 0.9 m deeper than that of TP-2S.

For a quantitative comparison, the total resistances at the total settlements of 12.7, 15.0, and 25.4 mm are summarized in Table 5. First, the total resistances at the s_T of 12.7 mm for the DPT-BC, DPT-AC, proposed method, and static load test were 2534, 3152, 3532, and 3463 kN, respectively. The total resistances at the s_T of 15.0 mm, were 2969, 3591, 4095, and 3904 kN for the DPT-BC, DPT-AC, this method, and static load test, respectively. The total resistances at the s_T of 25.4 mm were 5897 and 5662 kN for this method and static load test, respectively. The total resistances using the resistance combination method at the s_T of 12.7, 15.0, and 25.4 mm are greater than those using the static load test, because the hole depth of TP-2D was deeper than that of TP-2S by 0.9 m. In addition, the curing time of the cement paste was longer for TP-2D than TP-2S, as the DPT-AC of TP-2D and static load test of TP-2S were conducted 28 and 25 days, respectively, after pile installation as summarized in Table 1. Note that the load settlement curves of the DPT-BC and DPT-AC do not reach more than 25.4 mm.

For TP-2, the total resistances evaluated by the DPT-BC, DPT-AC, and proposed method are directly compared with those obtained from the static load tests as summarized in Table 5. The total resistances evaluated by the DPT-BC and DPT-AC are 73.2%–76.1% and 91.0%–92.0%, respectively, of those evaluated by the static load tests. Meanwhile, the total resistances evaluated by this method are 102.0%–104.9% of those evaluated by the static load tests. In other words, the total resistances evaluated using the proposed method are more similar to those obtained from the static load tests than those evaluated by the DPT-BC or DPT-AC. Fig. 12(b) and Table 5 show that the shape of the load–settlement curve and the total resistances evaluated using the proposed method in TP-2D, respectively, are similar to those obtained from the static load test in TP-2S.

6. Conclusions

In this study, a resistance combination method, which is based on the base resistance before curing of the cement paste and shaft resistance after curing of the cement paste of embedded piles, is developed. The load–settlement curve at the pile base estimated by the DPT conducted before curing of the cement paste (DPT-BC) and shaft resistance parameters estimated by the DPT conducted after curing of the cement paste (DPT-AC) are used for this method to estimate the load transfer curve and load–settlement curve at the pile head. The proposed method facilitates to obtain the combined load–settlement curve from the dynamic pile test (DPT) results.

Four pretensioned spun high strength concrete (PHC) piles were installed to investigate the load–settlement curves obtained using the resistance combination method. The diameters of TP-1 piles (TP-1D and TP-1S) were 600 mm, while those of TP-2 piles (TP-2D and TP-2S) were 500 mm. The lengths of the four test piles ranged from 12.3 to 13.9 m. The DPTs were performed before and after curing of the cement paste. The DPT-BC for both TP-1D and TP-2D piles was conducted using a drop hammer with the ram weight of 58.9 kN immediately after pile installation. The DPT-AC for both TP-1D and TP-2D piles were conducted using a hydraulic hammer with the ram weight of 98.1 kN 28–29 days after pile installation. Static load tests were conducted on TP-1S and TP-2S 21–25 days after pile installation. The load–settlement curves and corresponding resistances obtained by the proposed method of TP-1D and TP-2D were compared with those by the static load tests of TP-1S and TP-2S. The main observations of this study are as follows:

- The maximum total resistance and stiffness of the

combined load–settlement curve obtained by the resistance combination method are greater than those by the DPT-BC and DPT-AC.

- The shape of the combined load–settlement curve obtained by the proposed method is similar to that obtained by the static load test. Thus, the resistances evaluated by this method at the total settlements of 12.7, 15.0, and 25.4 mm approach those by the static load test.
- The resistance combination method may be widely applied in the dynamic pile tests for the effective estimation of the bearing capacity of embedded piles.
- The further studies are required to solve the limitations, which are not considered using the proposed method, including the inherent uncertainties in the CAPWAP analysis and the nonlinear behavior of embedded piles.

Acknowledgments

This work was supported by the Land and Housing Institute (LHI) research funded by the Korea Land and Housing Corporation (No. 2020-124) and the National Research Foundation of Korea (NRF) grant funded by the Korea government (MSIT) (No. NRF-2021R1A5A1032433).

References

AS-2159 (1995), Piling design and installation, Standards Association of Australia, Sydney, Australia.

ASTM D1143 (2013), Standard test methods for deep foundations under static axial compressive load, ASTM International, West Conshohocken, Pennsylvania, USA.

ASTM D4945 (2017), Standard test methods for high-strain dynamic testing of deep foundations, ASTM International, West Conshohocken, Pennsylvania, USA.

Coyle, H.M. and Reese, L.C. (1996), "Load transfer for axially loaded piles in clay", *J. Soil Mech. Found. Div.*, **92**(2), 1-26. https://doi.org/10.1061/JSFEAQ.0000850.

Fellenius, B.H. (1980), "The analysis of results from routine pile load tests", *Ground Eng.*, **13**(6), 19-31.

Han, K., Seo, M.J., Hong, W.T. and Lee, J.S. (2020), "End-bearing capacity of embedded piles with inclined-base plate: laboratory model tests", *J. Geotech. Geoenviron. Eng.*, **146**(8), 04020063. https://doi.org/10.1061/(ASCE)GT.1943-5606.0002304.

Hirayama, H. (1990), "Load–settlement analysis for bored piles using hyperbolic transfer functions", *Soils Found.*, **30**(1), 55-64. https://doi.org/10.3208/sandf1972.30.55.

Hong, W.P. and Chai, S.G. (2005), "Bearing capacity of the SDA pile in cohesive soil", *Proceedings of the 15th International Offshore and Polar Engineering Conference*, Seoul, Korea, June.

Hong, W.P. and Chai, S.G. (2003), "Skin friction capacity of SDA pile", *Proceedings of the 13th International Offshore and Polar Engineering Conference*, Honolulu, Hawaii, May.

Lashkari, A. (2013), "Prediction of the shaft resistance of nondisplacement piles in sand", *Int. J. Numer. Anal. Method. Geomech.*, **37**(8), 904-931. https://doi.org/10.1002/nag.1129.

Lee, J.S. and Park, Y.H. (2008), "Equivalent pile load-head settlement curve using a bi-directional pile load test", *Comput. Geotech.*, **35**(1), 124-133. https://doi.org/10.1016/j.compgeo.2007.06.008.

Li, L., Li, J., Sun, D. and Gong, W. (2017) "A semi-analytical approach for time-dependent load-settlement response of a jacked pile in clay strata", *Can. Geotech. J.*, **54**(12), 1682-1692. https://doi.org/10.1139/cgj-2016-0561.

Likins, G. and Rausche, F. (2004), "Correlation of CAPWAP with static load tests", *Proceedings of the 7th International Conference on the Application of Stress-wave Theory to Piles*, Kuala Lumpur, Malaysia, August.

Likins, G., Rausche, F., Thendean, G., and Svinkin, M. (1996), "CAPWAP correlation studies", *Proceedings of the 5th International Conference on the Application of Stress-wave Theory to Piles*, Orlando, Florida, September.

Mascarucci, Y., Miliziano, S. and Mandolini, A. (2014), "A numerical approach to estimate shaft friction of bored piles in sands", *Acta Geotechnica*, **9**(3), 547-560. https://doi.org/10.1007/s11440-014-0305-4.

Murakami, D.K. (2019), "A new concept of match quality of settlements for signal matching analysis on the dynamic pile testing", *Proceedings of the 10th International Conference on Stress Wave Theory and Testing Methods for Deep Foundations*, Lowell, Massachusetts, June.

Park, J.B. (2017), "A comparative study on the bearing capacity of dynamic load test and static load test of PHC bored pile", *J. Korean Geo-environmental Soc.*, **18**(9), 19-31.

Pile Dynamics Inc. (2014), CAPWAP background report version 2014, Pile Dynamics Inc., Cleveland, Ohio, USA.

Poulos, H.G. and Davis, E.H. (1968), "The settlement behaviour of single axially loaded incompressible piles and piers", *Geotechnique*, **18**, 351-371. https://doi.org/10.1680/geot.1968.18.3.351.

Randolph, M.F. and Wroth, C.P. (1978), "Analysis of deformation of vertically loaded piles", *J. Geotech. Eng. Div.*, **104**, 1465-1488. https://doi.org/10.1061/AJGEB6.0000729.

Rausche, F., Likins, G., Liang, L. and Hussein, M. (2010), "Static and dynamic models for CAPWAP signal matching", *Proceedings of the Art of Foundation Engineering Practice 2010*, West Palm Beach, Florida, February. https://doi.org/10.1061/41093(372)27.

Rollins, K.M., Clayton, R.J., Mikesell, R.C. and Blaise, B. (2005), "Drilled shaft side friction in gravelly soils", *J. Geotech. Geoenviron. Eng.*, **131**(8), 987-1003. https://doi.org/10.1061/(ASCE)1090-0241(2005)131:8(987).

Seo, M.J., Han, K., Park, J.B., Jeong, K.H. and Lee, J.S. (2021), "End bearing capacity of embedded piles with inclined base plate: Field dynamic and static tests", *Geomech. Eng.*, **26**(3), 261-274. https://doi.org/10.12989/gae.2021.26.3.261.

Seo, M., Park, J.B. and Lee, J.S. (2019), "Tip resistance characterization of embedded piles with inclined tip plates using dynamic tests", *Proceedings of the 16th Asian Regional Conference on Soil Mechanics and Geotechnical Engineering*, Taipei, Taiwan, October.

Terzaghi, K. and Peck, R. (1967), Soil mechanics in engineering practice, John Wiley, New York, USA.

Touma, F.T. and Reese, L.C. (1974), "Behaviors of bored piles in sand", *J. Geotech. Geoenviron. Eng.*, **100**7), 749-761. https://doi.org/10.1061/AJGEB6.0000065.

Woodward, R.J., Gardner, W.S. and Greer, D.M. (1972), Drilled pier foundations, McGraw-Hill, New York, USA.

Zhang, Q., Feng, R., Yu, Y., Liu, S. and Qian, J. (2019), "Simplified approach for prediction of nonlinear response of bored pile embedded in sand", *Soils Found.*, **59**(5), 1562-1578. https://doi.org/10.1016/j.sandf.2019.07.011.

GC

List of notations

i: segment number (e.g., Segment i)
j: loading step number (e.g., j-th loading step)
A_i: cross-sectional area of Segment i
B_i: bottom resistance of Segment i
$B_{i,j}$: bottom resistance of Segment i at the j-th loading step
E_i: elastic modulus of Segment i
k_i: soil stiffness of Segment i
L_i: length of Segment i
n_i: net settlement at the bottom of Segment i
$n_{i,j}$: net settlement at the bottom of Segment i at the j-th loading step
P_B: base resistance of the pile
$P_{B,j}$: pile base resistance at the j-th loading step
P_i: top resistance of Segment i
P_T: total load applied to the pile head
Q_B: base resistance
q_B: unit base resistance
Q_{BA}: base resistance evaluated by the DPT conducted after curing of the cement paste (DPT-AC)
Q_{BB}: base resistance evaluated by the DPT conducted before curing of the cement paste (DPT-BC)
q_i: shaft quake of Segment i
Q_S: shaft resistance
q_S: unit shaft resistance
Q_{SA}: shaft resistance evaluated by the DPT-AC
Q_{SB}: shaft resistance evaluated by the DPT-BC
Q_T: total resistance
Q_{TA}: total resistance evaluated by the DPT-AC
Q_{TB}: total resistance evaluated by the DPT-BC
Q_{TC}: total resistance evaluated by the combination method
s_B: base settlement of the pile
$s_{B,j}$: pile base settlement at the j-th loading step
SF_i: shaft resistance of Segment i
$(SF_i)_u$: ultimate shaft resistance of Segment i
s_i: top settlement of Segment i
s_T: total settlement at the pile head
δ_i: elastic deformation of Segment i